THE JOURNAL OF BIOLOGICAL CHEMISTRY
Vol. 275, No. 46, Issue of November 17, pp. 35932–35941, 2000

Printed in U.S.A.

In Vivo Quantification of Parallel and Bidirectional Fluxes in the Anaplerosis of *Corynebacterium glutamicum**

Received for publication, October 27, 1999, and in revised form, May 15, 2000
Published, JBC Papers in Press, August 16, 2000, DOI 10.1074/jbc.M908728199

Sören Petersen, Albert A. de Graaf‡, Lothar Eggeling, Michael Möllney§, Wolfgang Wiechert§, and Hermann Sahm

From the Institut für Biotechnologie 1, Forschungszentrum Jülich GmbH, 52425 Jülich, Germany and §Institut für Mechanik und Regelungstechnik, Universität-GH Siegen, 57068 Siegen, Germany

The C_3-C_4 metabolite interconversion at the anaplerotic node in many microorganisms involves a complex set of reactions. C_3 carboxylation to oxaloacetate can originate from phosphoenolpyruvate and pyruvate, and at the same time multiple C_4-decarboxylating enzymes may be present. The functions of such parallel reactions are not yet fully understood. Using a ^{13}C NMR-based strategy, we here quantify the individual fluxes at the anaplerotic node of *Corynebacterium glutamicum*, which is an example of a bacterium possessing multiple carboxylation and decarboxylation reactions. *C. glutamicum* was grown with a ^{13}C-labeled glucose isotopomer mixture as the main carbon source and ^{13}C-labeled lactate as a cosubstrate. 58 isotopomers as well as 15 positional labels of biomass compounds were quantified. Applying a generally applicable mathematical model to include metabolite mass and carbon labeling balances, it is shown that pyruvate carboxylase contributed 91 ± 7% to C_3 carboxylation. The total *in vivo* carboxylation rate of 1.28 ± 0.14 mmol/g dry weight/h exceeds the demand of carboxylated metabolites for biosyntheses 3-fold. Excess oxaloacetate was recycled to phosphoenolpyruvate by phosphoenolpyruvate carboxykinase. This shows that the reactions at the anaplerotic node might serve additional purposes other than only providing C_4 metabolites for biosynthesis.

The interconversions between the C_3 metabolism and the C_4 metabolites of the tricarboxylic acid cycle function either as a replenishment of tricarboxylic acid cycle intermediates (anaplerosis) or as the initial steps of gluconeogenesis. These carboxylation and decarboxylation reactions are catalyzed by a number of enzymes (1, 2). Synthesis of oxaloacetate via carboxylation of C_3 metabolites may be catalyzed by phosphoenolpyruvate (PEP)[1] carboxylase, PEP carboxytransphosphorylase, or pyruvate carboxylase. The reverse reaction, decarboxylation of oxaloacetate, may analogously lead to PEP or pyruvate, catalyzed by PEP carboxykinase or oxaloacetate decarboxylase, respectively. NAD^+- or $NADP^+$-dependent malic enzyme catalyzes the reaction from malate to pyruvate. In some organisms, this enzyme is also thought to act in a pyruvate-carboxylating sense (3).

To date, a full understanding of these enzymatic reactions and their functions has been hindered by a lack of knowledge about their activities *in vivo*. The occurrence of parallel reactions and the involvement of a set of metabolites in activity control of the enzymes prevents reliable estimations on the actual enzyme use. Moreover, it is not possible to derive quantitative data on *in vivo* flux rates by enzyme characterizations alone. Instead, carbon-13 labeling techniques, which employed NMR spectroscopy (for an overview, see *e.g.* Refs. 4 and 5) or mass spectrometry, as well as carbon-14 radiolabeling methods have been used to quantify *in vivo* intracellular fluxes in central metabolism including conversions between PEP, pyruvate, and oxaloacetate/malate. However, although these studies quantified the total C_3 carboxylation and C_4 decarboxylation rates, they either investigated cases in which only a single flux in each direction had to be considered (*e.g.* 6–10), in which parallel reactions were lumped together (11, 12), or in which the resolution of parallel reactions required assumptions on compartmentation (13, 14). For the parallel decarboxylating reactions in *Bacillus subtilis*, it was possible to derive separate upper bounds (15). One study estimated the relative carboxylation fluxes originating from PEP and pyruvate in *Corynebacterium glutamicum* based on comparison of deletion mutants (16), an approach that, however, by itself does not represent the natural situation, since fluxes are severely disturbed in mutants and the cell may react very flexibly (17, 18).

In this study, we present and apply a strategy for the resolution of the bidirectional as well as multiply parallel enzymatic conversions within anaplerosis that is generally applicable to a variety of biological systems. The experimental approach is based on ^{13}C labeling techniques and NMR spectroscopy and makes full use of the recently found explicit mathematical solution of isotopomer balances (19) and the accompanying experimental design framework (20). The procedure was applied to *C. glutamicum*, since this organism possesses PEP and pyruvate carboxylases, PEP carboxykinase, oxaloacetate decarboxylase, and $NADP^+$-dependent malic enzyme, which are all shown to be active *in vitro* (21–30). Previous work on flux distribution in this organism suggests that both carboxylation and decarboxylation might occur simultaneously *in vivo* (17, 18).

EXPERIMENTAL PROCEDURES

Cultivation and ^{13}C Stable Isotope Label Application—C. glutamicum wild type ATCC 13032 was pregrown overnight in 100 ml of 3.7% brain-heart-glucose bouillon (Difco), washed twice with buffer of 50 mM Tris·HCl and 50 mM NaCl, pH set to 6.8 using NaOH, and inoculated into the bioreactor containing unlabeled medium to result in an optical density at 600 nm (A_{600}) of approximately 1.1.

Cultivation was carried out in a KLF2000 bioreactor (Bioengineering, Wald, Switzerland) equipped with an automatic medium feeding system YFC 01Z (Sartorius, Göttingen, Germany) and a COI online

* This work was supported by Degussa-Hüls AG. The costs of publication of this article were defrayed in part by the payment of page charges. This article must therefore be hereby marked "*advertisement*" in accordance with 18 U.S.C. Section 1734 solely to indicate this fact.

‡ To whom correspondence should be addressed. Tel.: 49-2461-613969; Fax: 49-2461-612710; E-mail: a.de.graaf@fz-juelich.de.

[1] The abbreviations used are: PEP, phosphoenolpyruvate; AcCoA, acetyl coenzyme A; αKG, α-ketoglutarate; OAA, oxaloacetate; Pyr, pyruvate; TriP, triose phosphates.

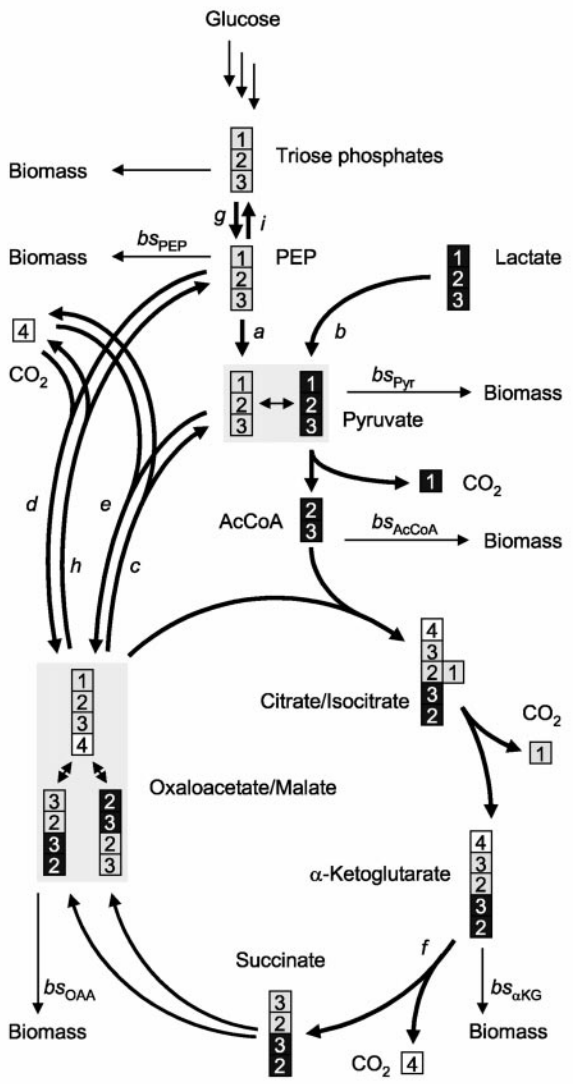

FIG. 1. **Simplified metabolic network and carbon atom transitions used in anaplerotic flux estimation.** The symbols *a*--*i* refer to the derivation of central metabolic fluxes. The enzymatic correlations are as follows: pyruvate kinase and phosphotransferase system for glucose uptake (*a*); L-lactate dehydrogenase (*b*); oxaloacetate decarboxylase and malic enzyme (*c*); PEP carboxylase (*d*); pyruvate carboxylase (*e*); α-ketoglutarate dehydrogenase complex, succinyl coenzyme A synthetase, succinate dehydrogenase, and fumarase (*f*); glyceraldehyde 3-phosphate dehydrogenase, phosphoglycerate kinase, phosphoglyceromutase, and enolase (*g* and *i*); PEP carboxykinase (*h*). Precursor requirements for biomass synthesis are denoted by *bs*. Metabolites that do not represent branch points are left out for simplicity, and pools of metabolites for which near equilibrium conditions are assumed (*i.e.* the triose phosphates (dihydroxyacetone phosphate and glyceraldehyde 3-phosphate) (2), citrate/isocitrate, and oxaloacetate/malate (11)) are each lumped together.

exhaust gas $^{13}CO_2/^{12}CO_2$ monitor (Fischer Analysen Instrumente, Leipzig, Germany). The medium was based on an optimization described (31) and consisted of 10 g/liter $(NH_4)_2SO_4$, 0.5 g/liter K_2HPO_4, 0.5 g/liter KH_2PO_4, 0.5 g/liter NaCl, 0.285 g/liter $MgSO_4 \cdot 7H_2O$, 0.05 g/liter $CaCl_2 \cdot 2H_2O$, 28.5 mg/liter $FeSO_4 \cdot 7H_2O$, 11.2 mg/liter $MnSO_4 \cdot H_2O$, 763 μg/liter $CuSO_4 \cdot 5H_2O$, 6.3 mg/liter $ZnSO_4 \cdot 7H_2O$, 130 μg/liter $CoCl_2 \cdot 6H_2O$, 43 μg/liter $NiCl_2 \cdot 6H_2O$, 65 μg/liter $Na_2MoO_4 \cdot 2H_2O$, 28 μg/liter $AlK(SO_4)_2 \cdot 12H_2O$, 20 μg/liter $Na_2SeO_3 \cdot 5H_2O$, 50 μg/liter H_3BO_3, 0.85 mg/liter biotin, 0.1 g/liter EDTA·2Na·$2H_2O$, and 0.02% polypropylene glycol P1200 as antifoam agent. The medium was supplemented with either unlabeled carbon sources (21 mM glucose and 4 mM sodium-L-lactate) or a mixture of isotopically enriched substrates containing 4.2 mM [1-^{13}C]glucose and 2.1 mM [$^{13}C_6$]glucose (both from Cambridge Isotope Laboratories, Andover, MA), 14.7 mM unlabeled glucose, and 4 mM sodium L-[3-^{13}C]lactate (Euriso-top, Gif-sur-Yvette, France). This optimal isotopomeric substrate composition was evaluated by computer simulations using the metabolic flux model described below and the experimental design procedures outlined in Ref. 20.

Culture pH was automatically maintained at 6.8 by a dosage of 2 N NaOH. The culture volume was controlled at 600 ml by weight measurement and culture broth withdrawal. Peristaltic pumps were used for all liquid flows. Cultivation temperature was 30 °C. Aeration was achieved by synthetic air (80% N_2 and 20% O_2) at a flow rate of 46 liter/h and 1200 rpm stirrer speed. The oxygen partial pressure was measured but not controlled.

Five hours after inoculation of the bioreactor, the carbon source was consumed, as could be monitored via respiration activity, and the continuous chemostat mode was started with a dilution rate of 0.1 h^{-1}, *i.e.* 60 ml/h feed of unlabeled medium. At a cultivation time of 55 h, the respiration activity and A_{600} was stabilized and remained constant for an additional 42 h. Oxygen partial pressure was constant at approximately 80% of air saturation. Metabolic steady-state conditions thus established, the unlabeled feed was replaced by labeled medium as described above. After 29 h of subsequent cultivation, the biomass was harvested, washed twice, and freeze-dried.

Analytical Methods—The optical density (A_{600}) of culture samples was measured on a UV 160A spectrophotometer (Shimadzu, Tokyo, Japan). Samples were diluted to a resulting A_{600} between 0.1 and 0.3 prior to measurements. Culture supernatants were analyzed for glucose, L-lactate, and ammonia using enzymatic test kits (Roche Molecular Biochemicals). Carbon and nitrogen contents of freeze-dried biomass were determined using a CHNS 932 element analyzer (Leco, St. Joseph, MI).

NMR Spectroscopy—Carbon-13 labeling patterns of metabolites isolated from labeled cell material (*i.e.* not from the cytoplasm) were determined by NMR spectroscopy. To this end, 250 mg of freeze-dried cells was hydrolyzed in 12 ml of 6.0 N HCl for 12 h at 105 °C. One half of the hydrolysate was used for two-dimensional NMR measurements (see below), the other half for fractionation of proteinogenic amino acids by cation exchange chromatography as described previously (11, 32). Amino acid fractions of alanine, aspartate, glutamate, glycine, lysine, phenylalanine, serine, threonine, and valine as well as the remaining cell hydrolysate were each lyophilized, redissolved in 700 μl of deuterium oxide (Deutero, Kastellaun, Germany) containing 2 mM of sodium trimethylsilylpropionate-2,2,3,3-d_4 (Aldrich), and filled into 5-mm NMR sample tubes. All NMR measurements were carried out on a Bruker AMX400-WB spectrometer system at 400.13 MHz for ^{1}H and 100.61 MHz for ^{13}C.

Isotopomer distributions in amino acids were determined from ^{13}C spectra acquired under continuous composite pulse broadband decoupling using a 70° pulse, a sweep width of 26.3 kHz, and a repetition time of 2 s. 25,600 scans of 32,768 complex points were accumulated per spectrum. Fractional ^{13}C enrichments of protonated carbon atoms were determined by proton-^{13}C decoupling difference spectroscopy as previously published (11, 32, 33). To access labeling patterns in glycerol, a heteronuclear single-quantum correlated two-dimensional spectrum (34) was recorded from the sample containing the complete cell hydrolysate. The acquisition parameters were t_{1max} = 520 ms, t_{2max} = 231 ms, data size before zero-filling 3072 points in t_1 and 2048 points in t_2. Sweep width was 4.42 kHz for ^{1}H and 2.95 kHz for ^{13}C; the carrier position was 4.8 ppm for ^{1}H and 63.1 ppm for ^{13}C. Total recording time was 53.5 h.

RESULTS

Labeled Substrate Mixture for Optimal Resolution of the Anaplerotic Fluxes—Fig. 1 depicts the subnetwork of central metabolism relevant for resolution of the anaplerotic fluxes, along with the carbon atom transitions. It essentially comprises the tricarboxylic acid cycle, anaplerotic reactions, and the conversions of triose phosphates via PEP and pyruvate to acetyl coenzyme A. The glyoxylate cycle is not considered, since it is not active during growth of *C. glutamicum* on glucose as we have shown in previous ^{13}C labeling studies (11, 18, 35). ^{13}C fractional enrichments and isotopomer distributions of biomass precursors from this part of central metabolism can be determined by NMR measurements of glycerol and the proteinogenic amino acids alanine, aspartate, glutamate, phenylalanine, serine, and threonine from a biomass hydrolysate. Previous experiments employing [1-^{13}C]glucose as the sole labeled substrate enabled a detailed and accurate flux analysis in *C. glutamicum*

TABLE I

Labeling patterns of central metabolites relevant to anaplerosis and tricarboxylic acid cycle flux estimation

Shown are NMR measurements and, in parentheses, simulated values based on the mathematical model solution outlined in the Appendix. Biomass compounds from which ^{13}C fine structures were determined are underlined (*cf.* the illustration of ^{13}C signal fine structures in Fig. 2). See Tables A-II and A-III in the Appendix for measurement accuracies. ND, not determinable.

Central metabolite and carbon atom position	Measured from biomass compound	^{13}C fractional enrichment	Fine structure of ^{13}C multiplet signal (%)			
			s	d_{-1}	d_{+1}	*dd*
		%				
Triose phosphates C-2	Glycerol C-2	ND (11.3)	14.5 (14.6)	15.6[a] (15.1)		69.9 (70.3)
Phosphoenolpyruvate C-2	Phe C-2	12.2 (12.3)	21.4 (22.5)	7.7 (8.4)	10.9 (11.9)	60.0 (57.1)
Phosphoenolpyruvate C-3	Phe C-3	19.9 (20.0)	51.5 (50.4)	35.7 (37.3)	7.5 (7.1)	5.3 (5.2)
Pyruvate C-2	Ala C-2	11.6 (11.5)	22.3 (22.4)	8.6 (8.4)	12.2 (12.5)	56.9 (56.7)
Pyruvate C-3	Ala C-3, Glu C-4	26.2 (25.8)	67.2 (69.2)	32.8 (30.8)		
Oxaloacetate C-2	Asp C-2, Glu C-3	15.4 (15.8)	41.2 (40.9)	18.4 (19.2)	13.8 (13.0)	26.6 (26.9)
Oxaloacetate C-3	Asp C-3, Thr C-3, Glu C-2	23.2 (23.1)	56.4 (55.9)	21.0 (21.4)	16.5 (16.7)	6.1 (6.0)
α-Ketoglutarate C-3	Glu C-3	15.4 (15.8)	43.7 (44.5)	46.0[b] (45.2)		10.3 (10.3)
α-Ketoglutarate C-4	Glu C-4, Ala C-3	26.1 (25.8)	58.4 (58.2)	11.9 (11.0)	24.6 (25.9)	5.1 (4.9)

[a] Since glycerol is a symmetrical molecule, only the sum of d_{-1} and d_{+1} is determinable.
[b] Due to overlapping peaks, the sum of d_{-1} and d_{+1} is given.

but did not allow us to discriminate between PEP- and pyruvate-involving fluxes because fractional enrichments of PEP and pyruvate were found to be identical (11). Therefore, in our present experiment, [3-^{13}C]lactate was used as a labeled cosubstrate to result in a differently labeled pyruvate pool. Furthermore, we additionally used uniformly labeled [$^{13}C_6$]glucose against a background of unlabeled glucose, since this approach allows to estimate the fractions of the PEP and pyruvate pools that originate from oxaloacetate (15, 34). Thus, in this study, an optimized substrate mixture of the four species [1-^{13}C]glucose, [$^{13}C_6$]glucose, unlabeled glucose, and L-[3-^{13}C]lactate was employed in a single experiment.

Extracellular Flux Rates—Extracellular fluxes (*i.e.* between the cells and the surrounding medium) were determined to normalize the metabolic network and to check the consistency of the cultivation data. From three samples taken during steady state of the culture, the dry weight obtained was 1.86 ± 0.03 g/liter. The remaining concentrations of glucose and lactate were 0.014 ± 0.003 and 0.06 ± 0.01 mM, respectively. Ammonia concentration was 139 ± 1 mM. From these measurements, feed concentrations, and the dilution rate, the specific uptake rates were calculated as 1.13 ± 0.02 mmol of glucose/g dry weight/h, 0.21 ± 0.01 mmol/g/h lactate, and 0.65 ± 0.05 mmol/g/h ammonia. Carbon dioxide concentrations measured in the exhaust gas were 1726 ± 38 ppm of $^{12}CO_2$ and 292 ± 6 ppm of $^{13}CO_2$ (molar fractions), corresponding to a specific carbon dioxide production rate of 3.73 ± 0.15 mmol/g/h. Total carbon and nitrogen contents of dry biomass were 41.4 ± 0.6 and 9.7 ± 0.2%, respectively. Except for small amounts of alanine and valine detected by NMR (<0.1 mM, *i.e.* less than 0.5% of the carbon balance), no other products or compounds (*e.g.* protein that could indicate cell lysis) were present in the culture supernatant. Hence, the element balances for carbon and nitrogen are closed within the experimental error margins (97 ± 4 and 106 ± 8%, respectively).

NMR Quantifications—Fractional enrichments and/or ^{13}C spectral fine structures were determined from a total of 24 carbon atoms in the nine purified amino acids listed under "Experimental Procedures." Moreover, the ^{13}C fine structures of glycerol were evaluated from the two-dimensional spectrum of the cell hydrolysate by means of cross-sections through the maxima of the ^{13}C signals. The metabolic and isotopic steady state labeling data derived from these measurements for the precursor metabolites triose phosphates, PEP, pyruvate, oxaloacetate, and α-ketoglutarate are summarized in Table I, while Fig. 2 shows the relevant NMR spectra. In the following, we will show how these data can be used in a simple and intuitive approach employing basic carbon-13 and isotopomer balances to analyze the network depicted in Fig. 1. The results of the comprehensive computer-based flux analysis based on the full set of NMR data, together with the description of the metabolic model used, are given in the Appendix. Results of this comprehensive analysis that are relevant for the network of Fig. 1 are included in Table I for comparison.

Pyruvate Formation from Oxaloacetate Is a Minor Route—As can be seen from Fig. 3*A*, fluxes leading to pyruvate originate from PEP (*a*), the cosubstrate lactate (*b*), or oxaloacetate/malate (*c*). For the fractional enrichments in carbon positions 2 and 3 of pyruvate, the label balances at metabolic and isotopic steady state can be set up (Fig. 3*A*) as follows,

$$(a + b + c)FE_{\mathrm{Pyr,C\text{-}2}} = a \cdot FE_{\mathrm{PEP,C\text{-}2}} + b \cdot FE_{\mathrm{Lact,C\text{-}2}} + c \cdot FE_{\mathrm{OAA,C\text{-}2}} \quad \text{(Eq. 1)}$$

$$(a + b + c)FE_{\mathrm{Pyr,C\text{-}3}} = a \cdot FE_{\mathrm{PEP,C\text{-}3}} + b \cdot FE_{\mathrm{Lact,C\text{-}3}} + c \cdot FE_{\mathrm{OAA,C\text{-}3}} \quad \text{(Eq. 2)}$$

where *FE* denotes the fractional enrichments in the specified position (available from measurements (Table I) or known in the case of the substrate lactate, which is fully labeled in C-3 and has natural ^{13}C abundance of 1.1% in the other carbons). Fractional labeling in each of the carbon atoms of pyruvate is therefore linearly dependent on the labels in the respective carbons of three metabolites and their relative fluxes leading into the pyruvate pool. The evaluation of Equations 1 and 2 with the data from Table I yields relative amounts of 85, 8, and 7% for *a*, *b* and *c*, respectively, as fractions of the total flux into the pyruvate pool. Since flux *b*, lactate consumption, was measured as 0.21 mmol/g/h, the other two fluxes can be directly assigned absolute values of $a = 2.23$ mmol/g/h (pyruvate kinase and phosphotransferase system for glucose uptake) and $c = 0.18$ mmol/g/h (oxaloacetate decarboxylase and/or malic enzyme). Thus, the first finding is that oxaloacetate decarboxylation contributed only little to pyruvate formation.

Oxaloacetate Is Predominantly Synthesized from Pyruvate—A set of equations analogous to those for the pyruvate node is obtained for the oxaloacetate/malate node (Fig. 3*B*),

$$(d + e + f)FE_{\mathrm{OAA,C\text{-}2}} = d \cdot FE_{\mathrm{PEP,C\text{-}2}} + e \cdot FE_{\mathrm{Pyr,C\text{-}2}} + f \cdot \tfrac{1}{2}\,(FE_{\alpha\mathrm{KG,C\text{-}3}} + FE_{\alpha\mathrm{KG,C\text{-}4}}) \quad \text{(Eq. 3)}$$

$$(d + e + f)FE_{\mathrm{OAA,C\text{-}3}} = d \cdot FE_{\mathrm{PEP,C\text{-}3}} + e \cdot FE_{\mathrm{Pyr,C\text{-}3}} + f \cdot \tfrac{1}{2}\,(FE_{\alpha\mathrm{KG,C\text{-}3}} + FE_{\alpha\mathrm{KG,C\text{-}4}}) \quad \text{(Eq. 4)}$$

where *d* represents PEP carboxylase, *e* represents pyruvate carboxylase, and *f* represents tricarboxylic acid cycle activity, and it is considered that both C-2 and C-3 of tricarboxylic acid cycle-derived oxaloacetate originate with equal probability

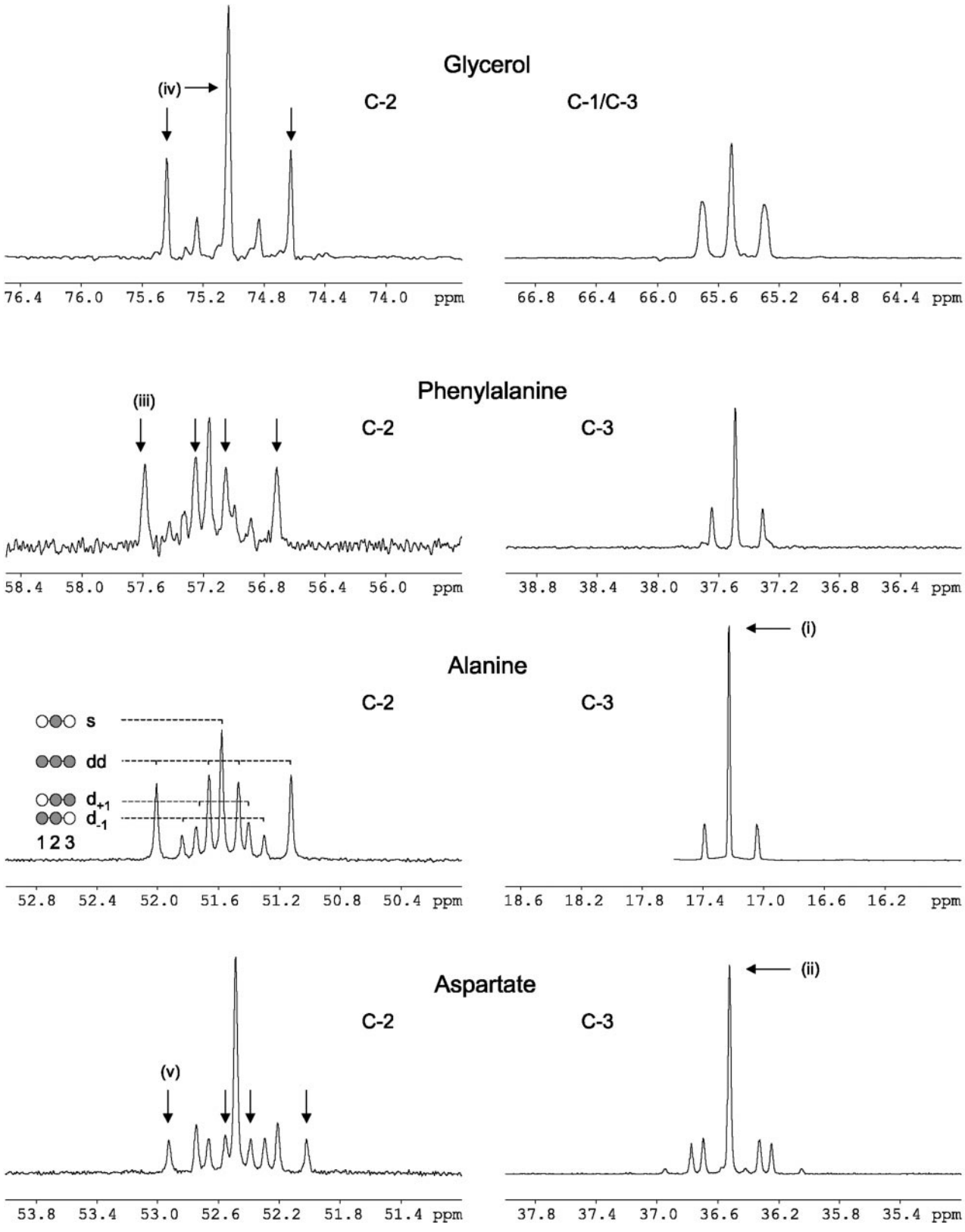

FIG. 2. **^{13}C-NMR spectra of compounds most relevant to anaplerotic flux estimation.** Signal fine structure composition is illustrated for the C-2 of alanine. Only molecules with a ^{13}C as the central carbon contribute to the multiplet signal. *s*, singlet peak of [2-^{13}C]alanine (no neighboring labels); d_{-1}, ^{13}C in the preceding position ([1,2-$^{13}C_2$]alanine) produces a doublet peak, split by scalar coupling; d_{+1}, ^{13}C in the following position ([2,3-$^{13}C_2$]alanine) yields another doublet split with a different coupling constant; *dd*, "doublet of doublet" signal of [$^{13}C_3$]alanine. Signals of terminal carbons only split into a singlet and one doublet. Influx of [3-^{13}C]lactate into pyruvate adds to the singlet peak of alanine C-3 (*i*). Because of pyruvate carboxylation, the label is also found in oxaloacetate, the precursor of aspartate (*ii*). In phenylalanine C-2, the *dd* fine structure of intact $^{13}C_3$ fragments is decreased (*iii*) in comparison with triose phosphates, measured through glycerol (*iv*). This is due to a back flux from oxaloacetate (see aspartate C-2; *v*) to PEP, the precursor of the phenylalanine aliphatic moiety. Note that in the symmetrical molecule of glycerol the $^{13}C_3$ isotopomer appears as a triplet instead of a doublet of doublets.

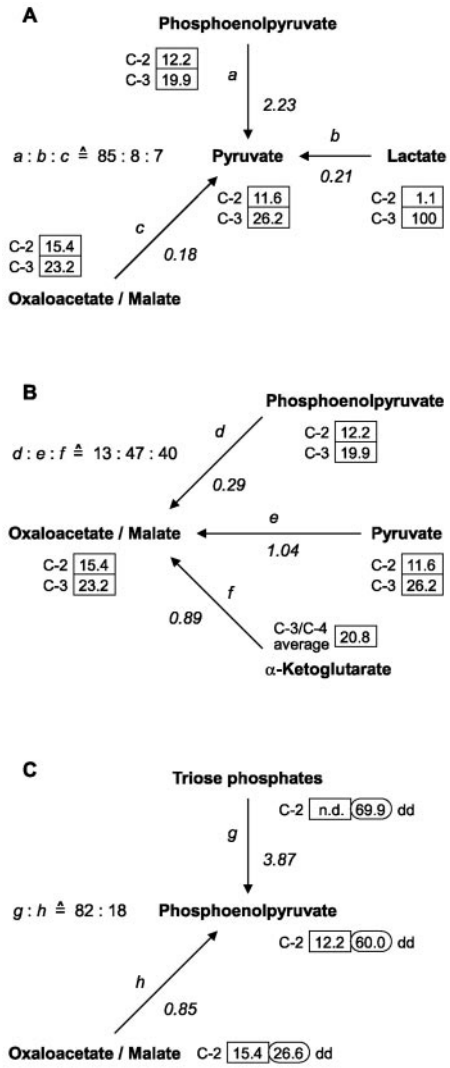

FIG. 3. **Metabolic nodes involved in anaplerotic flux distribution: pyruvate (*A*), oxaloacetate/malate (*B*), phosphoenolpyruvate (*C*).** For each node, the ratio of incoming fluxes is determinable from labeling data. *Rectangular boxes* represent measured ^{13}C fractional enrichments (in percent). *Ovals* indicate the intensities of the doublet of doublets fine structures as percentages of the total respective ^{13}C signals. See the legend to Fig. 1 for the enzymatic reactions corresponding to fluxes *a*--*g*. Flux rate estimates are given in mmol/g dry weight/h (*italic numbers*).

from C-3 and C-4 of α-ketoglutarate due to label scrambling at the symmetrical molecule of succinate. Since the label in the C-3 position of oxaloacetate is higher than that in C-3 of PEP and 2-oxoglutarate (Fig. 3*B*), it can be seen beforehand that oxaloacetate must have a high influx from pyruvate. With both Equations 3 and 4, and using the data in Table I, the relative fluxes *d*, *e*, and *f* are evaluated as 13, 47, and 40%, respectively, stating the second major result of the present investigation that the anaplerotic synthesis of oxaloacetate originates from pyruvate rather than PEP. This conclusion is visually perceivable from the ^{13}C spectra of C-3 of phenylalanine, alanine, and aspartate (Fig. 2), which show a high singlet contribution in oxaloacetate-derived aspartate C-3 similar to that in pyruvate-derived alanine C-3 rather than PEP-derived phenylalanine C-3. This illustrates that the supplementation of C-3-labeled lactate as cosubstrate enables the differentiation of PEP and pyruvate as possible origins of oxaloacetate, since the ensuing influx of [3-^{13}C]pyruvate caused the elevated singlet contribution in the C-3 signal of alanine. Thus, our data indicate that pyruvate carboxylase contributed at least 3-fold more to oxaloacetate synthesis than PEP carboxylase in *C. glutamicum*.

The Tricarboxylic Acid Cycle Is Drained by Decarboxylation of Oxaloacetate to Phosphoenolpyruvate—The phosphoenolpyruvate node, illustrated in Fig. 3*C*, involves PEP synthesis from triose phosphates (*g*) and by the back reaction from oxaloacetate to PEP (*h*). To date, no PEP synthase activity has been reported for *C. glutamicum*; hence, no influx to the PEP pool from pyruvate was considered.

Following the amount of intact $^{13}C_3$ fragments by inspection of the C-2 multiplet structure data of glycerol, phenylalanine, and aspartate (Fig. 2) reveals that a significant back flux from oxaloacetate to phosphoenolpyruvate must have been present. These triply labeled fragments, which appear as characteristic "doublet of doublet" (or as a triplet in the case of glycerol), fine structures in the C-2 NMR signals (Fig. 2), emerge from the portion of fully labeled glucose in the substrate mixture. Their relative amount (Table I), as a fraction of the total ^{13}C signal, is highest in triose phosphates (69.9%) and significantly lower in PEP (60.0%), an observation that can only be explained by an influx to PEP from the pool of oxaloacetate, in which the amount of intact $^{13}C_3$ fragments is greatly reduced (26.6%) due to the reactions of the tricarboxylic acid cycle. As with the other nodes, a set of labeling equations is set up for the PEP node, now including isotopomers,

$$(g + h)FE_{\mathrm{PEP,C\text{-}2}} = g \cdot FE_{\mathrm{TriP,C\text{-}2}} + h \cdot FE_{\mathrm{OAA,C\text{-}2}} \quad \text{(Eq. 5)}$$

$$(g + h)FE_{\mathrm{PEP,C\text{-}2}} \cdot FS_{\mathrm{PEP,C\text{-}2}} = g \cdot FE_{\mathrm{TriP,C\text{-}2}} \cdot FS_{\mathrm{TriP,C\text{-}2}} + h \cdot FE_{\mathrm{OAA,C\text{-}2}} \cdot FS_{\mathrm{OAA,C\text{-}2}} \quad \text{(Eq. 6)}$$

where *FS* denotes the relative intensity of a fine structure within the ^{13}C signal of the position specified. Hence, the product of *FS* and the corresponding fractional enrichment (*FE*) is equal to an isotopomer fraction of a C_3 fragment. Using the "doublet of doublets" fine structures (Table I), the evaluation of Equations 5 and 6 yields a *g*:*h* flux ratio of 82:18 and an estimate of 11.5% for the fractional label in C-2 of triose phosphates ($FE_{\mathrm{TriP,C\text{-}2}}$) that was not measured. Thus, the third important result of this study is that the gluconeogenic enzyme PEP carboxykinase is strongly active in *C. glutamicum* even during growth on glucose.

Calculation of Absolute Flux Rates—So far, the relative influx distributions at the three nodes of the network (Fig. 1) have been derived separately. Now, by metabolite balancing, the absolute fluxes can be evaluated. First, a balance is formed for the pyruvate node,

$$a + b + c = e + f + bs_{\mathrm{Pyr}} + bs_{\mathrm{AcCoA}} + bs_{\alpha\mathrm{KG}} \quad \text{(Eq. 7)}$$

which takes into account the fact that all carbons leaving the pyruvate pool eventually arrive at oxaloacetate/malate, directly (*e*) or via the tricarboxylic acid cycle (*f*), or leave central metabolism as biosynthetic precursors, either directly from pyruvate or via acetyl coenzyme A and α-ketoglutarate, denoted by bs_{Pyr}, bs_{AcCoA}, and $bs_{\alpha\mathrm{KG}}$, respectively. A second balance considers that in steady state the anaplerotic net rate, *i.e.* carboxylating minus decarboxylating reactions, must equal the total anabolic demands of the tricarboxylic acid cycle intermediates oxaloacetate (bs_{OAA}) and α-ketoglutarate ($bs_{\alpha\mathrm{KG}}$).

$$d + e - (c + h) = bs_{\mathrm{OAA}} + bs_{\alpha\mathrm{KG}} \quad \text{(Eq. 8)}$$

Using the anabolic precursor demands at 0.1 h^{-1} growth rate ($bs_{\mathrm{PEP}} = 0.05$, $bs_{\mathrm{Pyr}} = 0.27$, $bs_{\mathrm{AcCoA}} = 0.29$, $bs_{\alpha\mathrm{KG}} = 0.13$, and $bs_{\mathrm{OAA}} = 0.17$ mmol g^{-1} h^{-1}; see Ref. 11 and Table A-I in the Appendix), the absolute fluxes are evaluated from the foregoing equations as $d = 0.29$, $e = 1.04$, $f = 0.89$, $g = 3.87$, and $h = 0.85$ mmol g^{-1} h^{-1}. Finally, a balance for the PEP node,

TABLE II

Fluxes in anaplerosis and adjoining parts of central metabolism in C. glutamicum grown carbon-limited at 0.1 h^{-1}

Comparison of estimates from a simplified metabolic subnetwork (Fig. 1) and a comprehensive mathematical model (see Appendix). 90% confidence intervals are shown for the results of the complete model. TCA, tricarboxylic acid.

Metabolic conversion	Flux estimates	
	From simplified subnet	From complete model (see Appendix)
	mmol g^{-1} h^{-1}	
Triose phosphates → PEP	3.87	4.1 ± 0.6[a]
PEP → triose phosphates	2.15	2.2 ± 0.6[a]
TCA cycle entry flux[b]	1.02	1.08 ± 0.12
PEP → pyruvate	2.23	2.61 ± 0.09
PEP → oxaloacetate	0.29	0.11 ± 0.09
Pyruvate → oxaloacetate	1.04	1.17 ± 0.11
Oxaloacetate → PEP	0.85	0.99 ± 0.09
Oxaloacetate/malate → pyruvate	0.18	<0.10
Glyoxylate shunt		<0.06

[a] The net rate from triose phosphates (via 3-phosphoglycerate) to PEP is more precisely identified as 1.91 ± 0.08 mmol g^{-1} h^{-1}.

[b] Oxaloacetate + acetyl coenzyme A → citrate/isocitrate.

$$g + h = a + d + i + bs_{PEP} \quad \text{(Eq. 9)}$$

reveals a back flux from PEP to triose phosphates (i) of 2.15 mmol/g/h that is due to near equilibrium conditions of the reactions between these metabolites (2, 11).

In Table II, the estimated fluxes in the network of Fig. 1 are summarized. Notably, these estimations were derived from a small set of NMR measurements, yet they show good consistency with the outcome of the complete mathematical model presented in the Appendix. The estimated contribution of PEP carboxylation to the total anaplerotic flux is higher using the simplified approach (0.29 mmol g^{-1} h^{-1}) than it is calculated based on the complete model (maximally 0.20 mmol g^{-1} h^{-1}), probably due to a partial exchange of oxaloacetate C-2 and C-3 labels by the reversible reactions between fumarate and oxaloacetate (36) that could only be properly considered in the complete, computer-based analysis. Labeling patterns simulated on the basis of the identified central metabolic fluxes using the complete model are shown in Table I along with the measured data. The modeled values are in very good agreement with the measurements, indicating the correctness of our modeling framework.

The validity of the results is further corroborated by the consistency of redundant NMR information as demonstrated in Table III for the anaplerotic reactions. Using the complete mathematical model, all anaplerotic and decarboxylating fluxes can be determined already, albeit with less precision, from the labeling patterns of only phenylalanine, alanine, and aspartate, which represent the three node metabolites phosphoenolpyruvate, pyruvate, and oxaloacetate, respectively. Due to the redundancy of labels in oxaloacetate and α-ketoglutarate, NMR information from glutamate can substitute for that from aspartate. Glycerol and serine substitute for phenylalanine because of the exchange between triose phosphates and phosphoenolpyruvate. Also, omission of alanine labeling information can be partly compensated by valine and glutamate. Even when the data from phenylalanine, alanine, and asparate are omitted altogether, the remaining information still suffices to reveal the principal findings that pyruvate carboxylation is the more active anaplerotic route and that PEP carboxykinase is simultaneously active *in vivo*. In neither case, NMR information subsets produce results that are statistically different from each other.

It should be noted that our results reflect overall fluxes in a bacterial population, which as a whole is in dynamic steady state, although its individual cells are growing and dividing. Thus, one may argue that, if different amino acids had been predominantly synthesized during different phases of the cell cycle with different flux situations, the flux estimates would depend on the choice of amino acids for labeling information. But this was clearly not the case (Table III). Moreover, if the system was not in metabolic and isotopic steady state, error ranges yielded by statistical analysis (20) would expand rather than decrease with an increasing number of otherwise redundant information, *i.e.* labeling data from different amino acids that are derived from the same intermediate. Again, such inconsistencies are not observed, and, as it is to be expected with truly redundant data, the best-confined confidence regions are in fact achieved with the full set of labeling data (Table II). This is in accordance with the finding that bacterial metabolism in balanced growth is practically unchanged throughout the cell cycle, except for the processes directly involved in DNA replication and cell division (37, 38).

In summary, the present results unequivocally show that pyruvate carboxylation is the main anaplerotic route with a contribution of 83% or greater to total anaplerotic activity, although *in vitro* data suggested pyruvate carboxylase is the less active enzyme compared with phosphoenolpyruvate carboxylase (24, 29). Anaplerotic gross rate and C_4 decarboxylation activities are 1.28 ± 0.14 and 0.99 ± 0.09 mmol/g dry weight/hour, respectively, with PEP carboxykinase catalyzing at least 90% of the decarboxylation flux. Thus, the activities of pyruvate kinase, pyruvate carboxylase, and PEP carboxykinase in *C. glutamicum* constitute an apparently futile substrate cycle via the metabolites PEP → pyruvate → oxaloacetate → PEP, with a net loss of one high energy phosphate bond per turn.

DISCUSSION

In vivo flux quantification is aimed at determining the actual flux through an enzyme-catalyzed reaction and reflects the flux through this reaction as integrated in the entirety of the cellular fluxes. A particularly attractive subset of metabolism is the interconversion of C_3 and C_4 units at the anaplerotic node. Here, in many organisms a set of enzymes is present, which are speculated to serve different purposes in linking glycolysis with biosynthesis demands (1). We have repeatedly quantified that in *C. glutamicum* in addition to a C_3-carboxylating forward flux a C_4-decarboxylating flux is present (11, 17, 18), and this condition is also found in *B. subtilis* (15).

In the present work, the resolution of forward, back, and parallel fluxes was accomplished in a single experiment by using a mixture of differently labeled carbon sources and subsequently reading out the labeling patterns of metabolic intermediates via amino acids from biomass protein. This approach is valid for dynamic steady state cultures of organisms with a virtually unchanged metabolism throughout the cell cycle, *i.e.* mostly bacteria (37, 38). In the present case of *C. glutamicum*, this key requirement is endorsed by the consistency of redundant NMR information from different biomass compounds leading back to the same central metabolite.

The results indicate that the reaction via pyruvate carboxylase constitutes the principal route of anaplerotic C_3 carboxylation in *C. glutamicum*, with a small but significant contribution by phosphoenolpyruvate carboxylase operating in a parallel sense. The pyruvate carboxylase is hard to detect *in vitro* (29). The situation is thus comparable with the flux via the α-ketoglutarate dehydrogenase, which based on *in vitro* enzyme studies was originally thought to be absent in *C. glutamicum*, but where NMR studies revealed its presence and actual use in the organism (39). The existence of two carboxylating enzymes is not limited to *C. glutamicum* alone, but occurs also in other bacteria (*e.g. Pseudomonas* (40, 41)),

TABLE III
Consistency and redundancy of NMR information

Anaplerotic flux identification by the complete mathematical model is not dependent on the choice of amino acids as source of labeling information as long as the relevant central metabolites are sufficiently represented. 90% confidence intervals are shown.

NMR data from compounds	Flux estimates				
	PEP → OAA	Pyruvate → OAA	OAA → PEP	OAA/malate → pyruvate	Glyoxylate shunt
			mmol g^{-1} h^{-1}		
Phe, Ala, Asp	<0.22	1.32 ± 0.20	1.02 ± 0.22	<0.12	<0.15
Phe, Ala, Glu	<0.29	1.21 ± 0.26	0.82 ± 0.30	<0.21	<0.23
Glycerol, Ser, Ala, Asp	<0.24	1.27 ± 0.31	0.95 ± 0.24	<0.33	<0.07
Glycerol, Ser, Ala, Glu	<0.34	1.18 ± 0.36	0.74 ± 0.28	<0.54	<0.14
Phe, Val, Asp, Glu	<0.22	1.29 ± 0.64	0.89 ± 0.16	<0.79	<0.16
All except Phe	<0.25	1.14 ± 0.19	0.97 ± 0.14	<0.18	<0.06
All except Ala	0.16 ± 0.11	1.10 ± 0.36	0.96 ± 0.11	<0.35	<0.09
All except Asp	0.18 ± 0.13	1.12 ± 0.15	1.01 ± 0.13	<0.11	<0.11
All except Phe, Ala, Asp	0.30 ± 0.19	0.78 ± 0.39	0.79 ± 0.19	<0.37	<0.14

whereas *B. subtilis* has exclusively the pyruvate carboxylase (42) and *Escherichia coli* the PEP carboxylase (43).

The presence of both enzymes might increase the flexibility of the organism under different environmental conditions. Interestingly, both enzymes of *C. glutamicum* exhibit different regulation properties. PEP carboxylase is inhibited by the oxaloacetate successor aspartate and activated by acetyl coenzyme A (44). For *C. glutamicum* ssp. *flavum*, an inhibition of PEP carboxylase by the tricarboxylic acid metabolites α-ketoglutarate, malate, and succinate has been shown (45). PEP carboxylase does not require ATP, so that its function is not directly dependent on the cell's energy charge. In contrast, pyruvate carboxylase needs ATP as a cosubstrate and is inhibited by AMP and ADP as well as by acetyl coenzyme A (29). Therefore, the presence and use of both reactions could be correlated with the ATP balance of the cell. Another possible reason for the existence of these parallel reactions might be different affinities of the two carboxylases to carbon dioxide or, more precisely, bicarbonate. In this case, anaplerotic fluxes would be influenced by bicarbonate concentration. Furthermore, pyruvate carboxylase is dependent on biotin as a prosthetic group (46), a cofactor for which *C. glutamicum* is auxotrophic. A PEP carboxylase-deficient mutant of *C. glutamicum* was shown to be considerably more dependent on biotin than the wild type when grown on glucose (29). Hence, the *in vivo* partitioning between PEP and pyruvate carboxylases might be correlated to biotin availability. In excess of biotin, PEP carboxylase-deficient mutants of *C. glutamicum* strains showed no significant alteration in growth and amino acid production when compared with their parental strains (24).

As a surprising result of the present flux analysis, anaplerotic carboxylations in *C. glutamicum* synthesize an excess of oxaloacetate, which is recycled by the reaction of phosphoenolpyruvate carboxykinase, effectively causing cycling between the cellular metabolite pools of pyruvate, oxaloacetate, and PEP. The cyclic flux is 3-fold in excess over the anaplerotic flux required for biosynthesis demands. Pyruvate recycling at rates of up to 3 times that of the tricarboxylic acid cycle has been reported before in liver cells (13, 14, 47). However, the substrate cycle detected in *C. glutamicum* stands in sharp contrast to bacterial model organisms such as *E. coli*, in which strict regulation keeps futile cycling at a minimum (48–50). In *E. coli*, the overexpression of both PEP carboxylase and PEP carboxykinase has a distinct negative effect on growth yield, which was interpreted as an obtruded cycle, which in this case would in fact be a futile cycle (50).

There is so far limited knowledge about anaplerotic cycling in bacteria. The C_4 decarboxylation flux quantified in this study may indeed be of fundamental physiological significance. The cycle detected could thus serve as an energy-consuming cycle (51). The inhibition of pyruvate carboxylase by ADP corresponds to this idea. We found during glutamate-producing conditions of *C. glutamicum* a low cyclic flux between C_3 and C_4 units of only half the anaplerotic net flux (17). This could therefore be attributed to a low energy charge and increased maintenance requirements due to the stress of biotin limitation under which the organism was grown to induce glutamate production. Another idea suggested is an assumed back flux from oxaloacetate via malate to pyruvate involving malate dehydrogenase and malic enzyme (26, 30). Together with pyruvate carboxylase, this cycle would constitute a transhydrogenase activity, generating NADPH from NADH and ATP. However, this cycle is definitely not operating under the conditions we used. Thus, the physiological function of the excessive cycling detected remains speculative unless a set of different flux situations can be compared. Cycling between fructose 6-phosphate and fructose 1,6-bisphosphate via phosphofructokinase and fructose 1,6-bisphosphatase is attributed a regulatory advantage, since a small effect on the rates of each of the two opposing reactions can produce a large change in the net flux (2). Thus, in general, the sum of the carboxylating and decarboxylating reactions apparently serves as a fine tuning within the central metabolism to balance the replenishing reactions with the catabolic reactions.

Acknowledgments—We thank D. Kownatzki and N. Isermann (University of Siegen) for contributions to the software tools for isotopomer network simulations and flux identification. Thanks are due to K. Striegel (Jülich) for expert technical assistance, to S. Grzesiek (Jülich) and D. Schipper (DSM, Delft), for help with two-dimensional NMR, and to W. Hilgers (Central Department of Analytical Chemistry of Forschungszentrum Jülich) for the elemental analysis of the biomass. We appreciate discussions with B. Eikmanns (University of Ulm) and A. Marx (Degussa-Hüls AG, Halle-Künsebeck). We are grateful to J. Carter-Sigglow for critical reading of the manuscript.

APPENDIX

Central Metabolic Flux Model and Flux Identification

Flux Model and Mathematical Methods—The determination of intracellular fluxes from labeling data was performed using the mathematical solution of carbon labeling systems introduced by Wiechert and co-workers (19, 20), which enables all stationary net fluxes in the *C. glutamicum* central metabolic carbon network to be quantified and at the same time quantifies the order of magnitude of most bidirectional fluxes. Unlike the original version (52, 53), which was exclusively based on ^{13}C fractional enrichments, the current-extended approach jointly processes both isotopomer spectral fine structure and fractional enrichment data.

The reaction scheme of central metabolism applied to this study is outlined in Fig. A-1. It is based on the framework previously applied by Marx *et al.* (11, 17, 18), the present

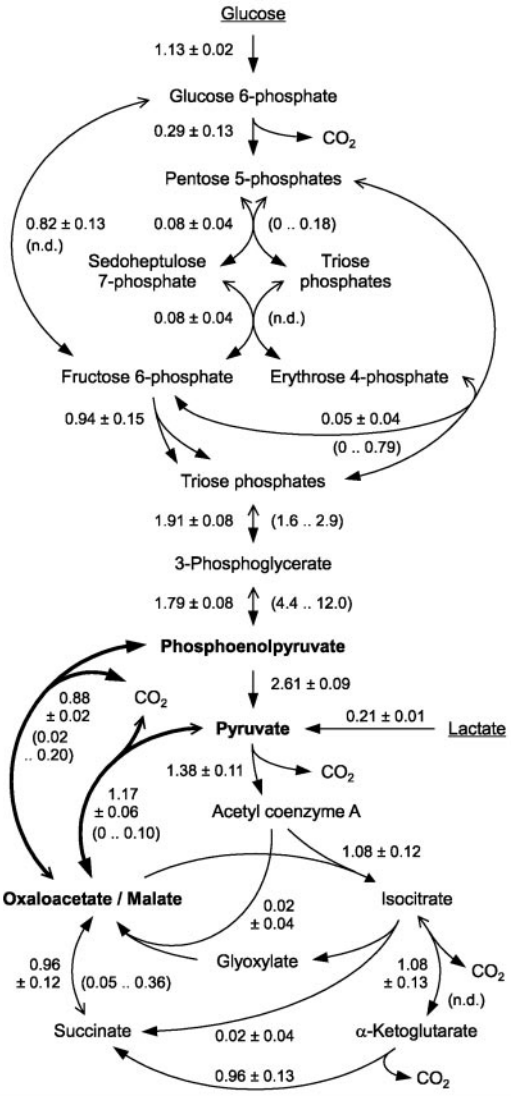

FIG. A-1. **Model framework of *C. glutamicum* central metabolism and intracellular fluxes determined for carbon-limited growth at 0.1 h^{-1}.** Uni- and bidirectional fluxes are represented by *single* and *double arrows*, respectively, with *solid arrows* indicating net directions. Net fluxes are shown as mean value ± S.E., and exchange fluxes (in *parentheses*) are shown as lower and upper bounds, both representing 90% confidence regions as yielded by statistical analysis (20). All fluxes are given in mmol/g dry weight/h. For clarity, the triose phosphate pool appears twice in the *figure*, and the effluxes of central metabolites for anabolic purposes (Table A-I) are not shown. *n.d.*, not determinable.

version taking into account multiple anaplerotic reactions. The carbon atom transitions of the central metabolic reactions as well as of the synthesis pathways of the amino acids that were used for NMR measurements, except for lysine, were taken from Refs. 34 and 53.

Assuming near equilibrium conditions, the various pentose 5-phosphate and the triose phosphate pools were each lumped together (17). Also, oxaloacetate and malate were modeled as one pool (11). Metabolites that do not represent branch points in the carbon flux net were not included in the model. Conversions that were treated as bidirectional included the transaldolase and transketolase reactions of the pentose phosphate pathway, the reaction of phosphoglucose isomerase, the enzymatic steps between triose phosphates and PEP (2), and those between succinate and malate (14, 36). The reaction of the $NADP^+$-dependent isocitrate dehydrogenase of *C. glutamicum*

TABLE A-I

Precursor fluxes into biomass synthesis at a growth rate of 0.1 h^{-1}

All anabolic fluxes are lumped together according to precursors in central metabolism. These fluxes were modeled as effluxes from the model network. Data were taken from Ref. 11.

Central metabolite	Required flux for biomass synthesis
	mmol g^{-1} h^{-1}
Acetyl-CoA	0.29
Erythrose 4-phosphate	0.03
Fructose 6-phosphate	0.01
Glucose 6-phosphate	0.02
Triose phosphates	0.01
α-Ketoglutarate	0.13
Oxaloacetate	0.17
Pentose 5-phosphates	0.09
Phosphoenolpyruvate	0.05
3-Phosphoglycerate	0.13
Pyruvate	0.27

TABLE A-II

^{13}C fractional enrichments measured by proton-^{13}C decoupling difference spectroscopy

Experimentally, 94.5% of isotopic equilibrium was reached based on first order wash-out kinetics and 2.9 residence times of cultivation on labeled substrate. The corrected values are extrapolated to full isotopic equilibrium as needed for mathematical modeling.

Amino acid	Carbon atom position	^{13}C enrichment		
		Measured	Corrected	Accuracy
		%	%	%
Alanine	2	11.0	11.6	±0.3
	3	24.0	25.3	±0.4
Aspartate	3	21.5	22.7	±0.4
Glutamate	2	22.1	23.3	±0.2
	3	14.6	15.4	±0.3
	4	25.3	26.7	±0.4
Lysine	3	19.2	20.3	±0.8
	6	12.1	12.8	±0.8
Phenylalanine	2	11.6	12.2	±0.4
	3	18.9	19.9	±1.6
	5, 9[a]	16.8	17.8	±0.4
	6, 7, 8[a]	9.0	9.5	±1.0
Serine	2	11.4	12.0	±0.4
Threonine	3	22.2	23.4	±1.4
	4	14.5	15.3	±0.4

[a] Average enrichment of specified carbon atoms.

(54) may also be reversible (8). The anaplerotic forward and back reactions were mathematically handled as two bidirectional steps: one between phosphoenolpyruvate and oxaloacetate/malate and the other between pyruvate and oxaloacetate/malate. The conversion of phosphoenolpyruvate to pyruvate was treated as unidirectional, since so far no PEP synthase activity has been found in *C. glutamicum* (44). Substrate uptake and all central metabolite precursor effluxes into biomass polymers were also set as unidirectional.

The model takes into account the fact that lysine biosynthesis in *C. glutamicum* is split into two branches, commonly called dehydrogenase and succinylase pathways (55). Label scrambling by implication of symmetric molecules had to be considered for the conversion of succinate via fumarate to malate, the synthesis of phenylalanine (2), and the succinylase pathway of lysine synthesis (32). Scrambling reactions were modeled as two parallel fluxes of equal size.

Fluxes for Biomass Synthesis—The data about precursor requirements for anabolic pathways (Table A-I) were originally obtained with a lysine-producing strain of *C. glutamicum* (11) that was derived from the wild type used in the present study by two mutagenesis steps (56). Their cellular compositions are thus comparable.

Labeling Data—The full sets of proton NMR (for ^{13}C fractional enrichments) and ^{13}C-NMR (for isotopomers) measure-

TABLE A-III
^{13}C NMR measurements

Total multiplet intensities for each specified carbon atom position are normalized as 100%. See Fig. 2 for signal components (s, d_{-1}, d_{+1}, and dd). Signals of terminal carbon atoms only split into s and d_{-1} or d_{+1}.

Compound	Carbon atom position	Signal			
		s	d_{-1}	d_{+1}	dd
		%	%	%	%
Alanine	2	22.3 ± 0.3	8.6 ± 0.3	12.2 ± 0.4	56.9 ± 0.4
	3	67.2 ± 1.0	32.8 ± 0.8		
Aspartate	2	41.2 ± 0.6	18.4 ± 0.5	13.8 ± 0.4	26.6 ± 0.7
	3	56.4 ± 0.3	21.0 ± 0.4	16.5 ± 0.3	6.1 ± 0.3
Glutamate	2	57.7 ± 1.4	16.9 ± 0.5	20.3 ± 0.5	5.1 ± 0.7
	3	43.7 ± 1.5	46.0 ± 1.4[a]		10.3 ± 1.0
	4	58.4 ± 0.6	11.9 ± 0.5	24.6 ± 0.4	5.1 ± 0.4
Glycerol	1[b]	41.0 ± 0.7		59.0 ± 0.8	
	2	14.5 ± 0.7	15.6 ± 0.4[a]		69.9 ± 1.1
Glycine	2	31.4 ± 0.3	68.6 ± 0.3		
Lysine	3	53.3 ± 0.6	43.1 ± 0.9[a]		3.6 ± 1.1
	4	43.5 ± 2.5	40.5 ± 2.2[a]		16.0 ± 3.2
	5	57.2 ± 1.9[c]	42.8 ± 3.6[a]		n.d.[c]
	6	41.7 ± 0.3	58.4 ± 0.7		
Phenylalanine	2	21.4 ± 0.8	7.7 ± 0.7	10.9 ± 0.9	60.0 ± 1.7
	3	51.5 ± 0.9	35.7 ± 0.7	7.5 ± 0.6	5.3 ± 0.6
Serine	2	20.2 ± 0.7	17.6 ± 0.7	11.1 ± 0.9	51.1 ± 2.1
Threonine	4	66.6 ± 0.3	33.4 ± 0.3		
Valine	4	68.5 ± 0.3	31.6 ± 0.5		
	5	88.0 ± 0.4	12.0 ± 0.6[d]		

[a] Sum of d_{-1} and d_{+1}; peaks overlap because of equal or nearly equal coupling constants.
[b] Values given for glycerol C-1 equal those of glycerol C-3 (symmetrical molecule).
[c] Sum of s and dd/2; dd was not determinable due to an insufficient signal to noise ratio.
[d] Coupling to carbon atom 3.

ments used in this work are presented in Tables A-II and A-III, respectively. The ^{13}C content determined in the bioreactor exhaust carbon dioxide of 14.5 ± 0.6% was taken as a fractional enrichment measurement of the culture CO_2 pool and fully integrated in the model.

Determination of Intracellular Fluxes—Using the mathematical framework described (19), fluxes in the central metabolism of *C. glutamicum* were identified by the best fit of simulated labeling data to the NMR measurements, *i.e.* by minimizing the sum of squared deviations between simulation and NMR data. These deviations were weighted according to measurement accuracy, so that equal ratios of model deviation to experimental error resulted in equal contributions to the sum of squares.

The directly determined specific rates of glucose and lactate uptake (1.13 and 0.21 mmol g^{-1} h^{-1}, respectively) as well as the anabolic effluxes of Table A-I were specified as constraints for flux fitting. Also, flux from PEP to pyruvate was constrained not to fall short of the glucose consumption rate, since this constitutes the minimum conversion dictated by glucose uptake via the phosphotransferase system (28, 57). The third carbon atom of serine was not considered for the least squares approach, since this position showed strong inconsistencies with the model, probably because of a back flux from glycine to serine via serine hydroxymethyl transferase (2).

The final outcome of the identified central metabolic fluxes, which was independent of starting values in the fitting process, is presented in Fig. A-I. The split ratio of lysine biosynthesis was 40 ± 5% dehydrogenase and 60 ± 5% succinylase pathways. The statistical analysis methods used to derive the specified error margins of the determined fluxes have been described elsewhere (20).

REFERENCES

1. Kornberg, H. L. (1966) in *Essays in Biochemistry* (Campbell, P. N., and Greville, G. D., eds) Vol. II, Academic Press, Inc., New York
2. Stryer, L. (1988) *Biochemistry*, 3rd Ed., W. H. Freeman Co., New York
3. Sundqvist, K. E., Hiltunen, J. K., Hassinen, I. E. (1989) *Biochem. J.* **257,** 913–916
4. Jeffrey, F. M. H., Rajagopal, A., Malloy, C. R., and Sherry, A. D. (1991) *Trends Biochem. Sci.* **16,** 5–10
5. Wiechert, W., and de Graaf, A. A. (1996) in *Advances in Biochemical Engineering Biotechnology* (Scheper, T., ed) Vol. 54, Springer-Verlag, Berlin
6. Raugi, G. J., Liang, T., and Blum, J. J. (1975) *J. Biol. Chem.* **250,** 5866–5876
7. Malloy, C. R., Sherry, A. D., and Jeffrey, F. M. H. (1988) *J. Biol. Chem.* **263,** 6964–6971
8. Des Rosiers, C., Fernandez, C. A., David, F., and Brunengraber, H. (1994) *J. Biol. Chem.* **269,** 27179–27182
9. Comte, B., Vincent, G., Bouchard, B., and Des Rosiers, C. (1997) *J. Biol. Chem.* **272,** 26117–26124
10. Comte, B., Vincent, G., Bouchard, B., Jetté, M., Cordeau, S., and Des Rosiers, C. (1997) *J. Biol. Chem.* **272,** 26125–26131
11. Marx, A., de Graaf, A. A., Wiechert, W., Eggeling, L, and Sahm, H. (1996) *Biotechnol. Bioeng.* **49,** 111–129
12. Jucker, B. M., Lee, J. Y., and Shulman, R. G. (1998) *J. Biol. Chem.* **273,** 12187–12194
13. Rabkin, M., and Blum, J. J. (1985) *Biochem. J.* **225,** 761–786
14. Baranyai, J. M., and Blum, J. J. (1989) *Biochem. J.* **258,** 121–140
15. Sauer, U., Hatzimanikatis, V., Bailey, J. E., Hochuli, M., Szyperski, T., and Wüthrich, K. (1997) *Nat. Biotechnol.* **15,** 448–452
16. Park, S. M., Shaw-Reid, C., Sinskey, A. J., and Stephanopoulos, G. (1997) *Appl. Microbiol. Biotechnol.* **47,** 430–440
17. Marx, A., Striegel, K., de Graaf, A. A., Sahm, H., and Eggeling, L. (1997) *Biotechnol. Bioeng.* **56,** 168–180
18. Marx, A., Eikmanns, B. J., Sahm, H., de Graaf, A. A., and Eggeling, L. (1999) *Metab. Eng.* **1,** 35–48
19. Wiechert, W., Möllney, M., Isermann, N., Wurzel, M., and de Graaf, A. A. (1999) *Biotechnol. Bioeng.* **66,** 69–85
20. Möllney, M., Wiechert, W., Kownatzki, D., and de Graaf, A. A. (1999) *Biotechnol. Bioeng.* **66,** 86–103
21. Shiio, I., and Ujigawa, K. (1978) *J. Biochem.* (*Tokyo*) **84,** 647–657
22. Eikmanns, B. J., Follettie, M. T., Griot, M. U., and Sinskey, A. J. (1989) *Mol. Gen. Genet.* **218,** 330–339
23. Jetten, M. S. M., and Sinskey, A. J. (1993) *FEMS Microbiol. Lett.* **111,** 183–188
24. Peters-Wendisch, P. G., Eikmanns, B. J., Thierbach, G., Bachmann, B., and Sahm, H. (1993) *FEMS Microbiol. Lett.* **112,** 269–274
25. Vallino, J. J., and Stephanopoulos, G. (1993) *Biotechnol. Bioeng.* **41,** 633–646
26. Cocaign-Bousquet, M., and Lindley, N. D. (1995) *Enzyme Microb. Technol.* **17,** 260–267
27. Jetten, M. S. M., and Sinskey, A. J. (1995) *Antonie Leeuwenhoek* **67,** 221–227
28. Cocaign-Bousquet, M., Guyonvarch, A., and Lindley, N. D. (1996) *Appl. Environ. Microbiol.* **62,** 429–436
29. Peters-Wendisch, P. G., Wendisch, V. F., Paul, S., Eikmanns, B. J., and Sahm, H. (1997) *Microbiology* **143,** 1095–1103
30. Dominguez, H., Rollin, C., Guyonvarch, A., Guerquin-Kern, J.-L., Cocaign-Bousquet, M., and Lindley, N. D. (1998) *Eur. J. Biochem.* **254,** 96–102
31. Weuster-Botz, D., Kelle, R., Frantzen, M., and Wandrey, C. (1997) *Biotechnol. Prog.* **13,** 387–393
32. Sonntag, K., Eggeling, L., de Graaf, A. A., and Sahm, H. (1993) *Eur. J. Biochem.* **213,** 1325–1331
33. Shaka, A. J., Barker, P. B., and Freeman, R. (1985) *J. Magn. Reson.* **64,** 547–552
34. Szyperski, T. (1995) *Eur. J. Biochem.* **232,** 433–448
35. Wendisch, V. F., Spies, M., Reinscheid, D. J., Schnicke, S., Sahm, H., and Eikmanns, B. J. (1997) *Arch. Microbiol.* **168,** 262–269

36. London, R. E., Allen, D. L., Gabel, S. A., and DeRose, E. F. (1999) *J. Bacteriol.* **181,** 3562–3570
37. Mandelstam, J., and McQuillen, K. (1973) *Biochemistry of Bacterial Growth*, 2nd Ed., Blackwell Scientific Publications, Oxford
38. Helmstetter, C. E. (1996) in *Escherichia coli and Salmonella* (Neidhardt, F. C., ed) 2nd Ed., Vol. 2, American Society for Microbiology Press, Washington, D. C.
39. Walker, T. E., Han, C. H., Kollman, V. H., London, R. E., and Matwiyoff, N. A. (1982) *J. Biol. Chem.* **257,** 1189–1195
40. Milrad de Forchetti, S. R., and Cazzulo, J. J. (1976) *J. Gen. Microbiol.* **93,** 75–81
41. O'Brien, R. W., Chuang, D. T., Taylor, B. L., and Utter, M. F. (1977) *J. Biol. Chem.* **252,** 1257–1263
42. Diesterhaft, M. D., and Freese, E. (1973) *J. Biol. Chem.* **248,** 6062–6070
43. Chao, Y.-P., and Liao, J. C. (1993) *Appl. Environ. Microbiol.* **59,** 4261–4265
44. Peters-Wendisch, P. G. (1996) *Anaplerotische Reaktionen in Corynebacterium glutamicum: Untersuchungen zur Bedeutung der PEP-Carboxylase und der Pyruvat-Carboxylase im Zentralstoffwechsel und bei der Aminosäure-Produktion*, Ph.D. thesis, University of Düsseldorf
45. Mori, M., and Shiio, I. (1985) *J. Biochem.* **98,** 1621–1630
46. Scrutton, M. C., and Young, M. R. (1972) in *The Enzymes* (Boyer, B. D., ed) Vol. 6, Academic Press, Inc., New York
47. Katz, J., Wals, P., and Lee, W.-N. P. (1993) *J. Biol. Chem.* **268,** 25509–25521
48. Chambost, J. P., and Fraenkel, D. G. (1980) *J. Biol. Chem.* **255,** 2867–2869
49. Daldal, F., and Fraenkel, D. G. (1983) *J. Bacteriol.* **153,** 390–394
50. Chao, Y.-P., and Liao, J. C. (1994) *J. Biol. Chem.* **269,** 5122–5126
51. Rognstad, R. (1996) *Biochem. Arch.* **12,** 71–83
52. Wiechert, W., and de Graaf, A. A. (1997) *Biotechnol. Bioeng.* **55,** 101–117
53. Wiechert, W., Siefke, C., de Graaf, A. A. (1997) *Biotechnol. Bioeng.* **55,** 118–135
54. Eikmanns, B. J., Rittmann, D., and Sahm, H. (1995) *J. Bacteriol.* **177,** 774–782
55. Schrumpf, B., Schwarzer, A., Kalinowski, J., Pühler, A., Eggeling, L., and Sahm, H. (1991) *J. Bacteriol.* **173,** 4510–4516
56. Schrumpf, B., Eggeling, L., and Sahm, H. (1992) *Appl. Microbiol. Biotechnol.* **37,** 566–571
57. Krämer, R. (1996) *J. Biotechnol.* **45,** 1–21